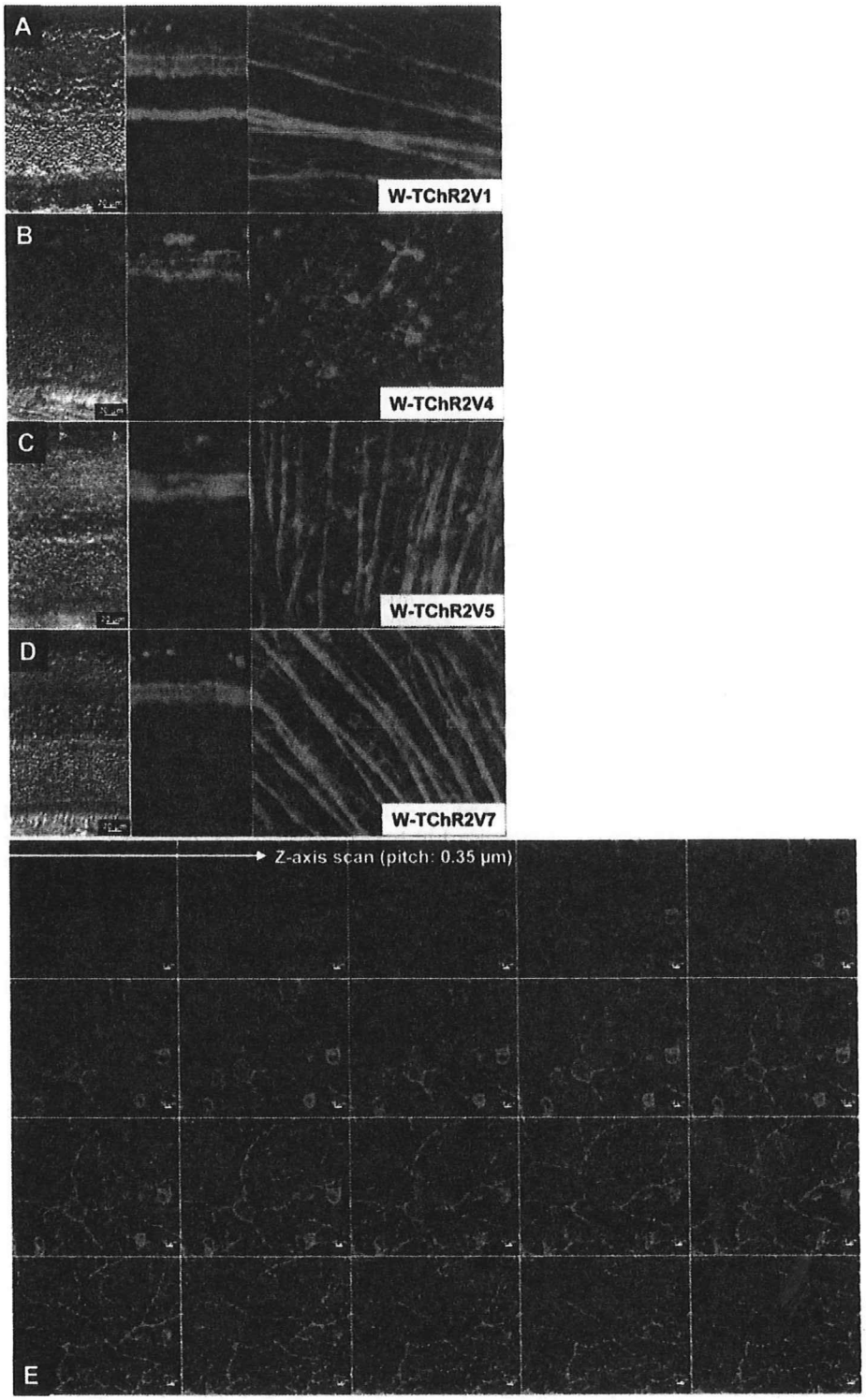

Figure 2. Microphotographs showing ChR2V expression in the inner retinal layers of each transgenic line. (A–D) The retinal organization of each transgenic line (A, W-TChR2V1; B, W-TChR2V4; C, W-TChR2V5; D, W-TChR2V7) showed normal features in the Nomarskii images (left). Fluorescence microphotography revealed various expression patterns in retinal slices (middle) and flat-mounted retinas (right). (E) Z-axis scan (pitch: 0.35 μm) images collected from a flat-mounted retina of a ChR2V+/− rat (line W-TChR2V4) showed that the ChR2V fluorescence (green) was coexpressed with fluorogold transported retrograde from the superior colliculus (blue).
doi:10.1371/journal.pone.0007679.g002

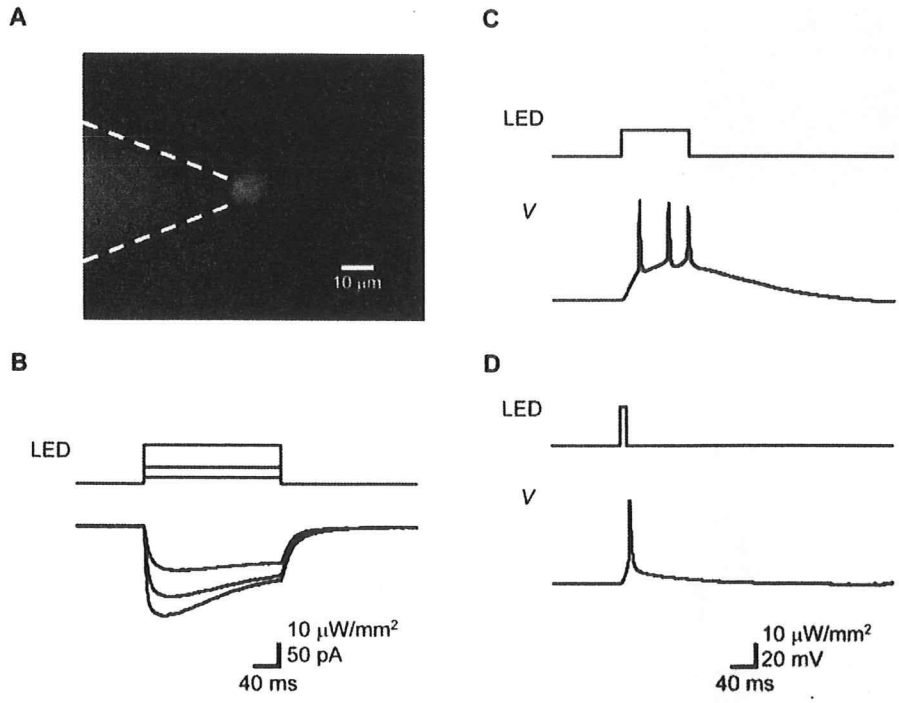

Figure 3. Direct photoactivation of ChR2V-expressing RGCs. (A) The blue light-emitting diode (LED)-evoked membrane currents and potentials were recorded under whole-cell recording from one of the ChR2V-expressing RGCs. (B) The photocurrents and their dependency in the LED power density. (C–D) The membrane potential responses of a ChR2V-expressing RGC to LED pulses of 100-ms (C) or 10-ms (D) duration.
doi:10.1371/journal.pone.0007679.g003

observed in rodents without retinal degeneration [22] and indicates that the ectopic expression of ChR2V did not affect retinal structure (Fig. 4A, B). After continuous toxic light exposure, the cells in the ONL were almost absent in both the superior and inferior retinas from both the ChR2V−/− (Fig. 4C) and ChR2V+/− rats (Fig. 4D). The disappearance of the ONL was also noted under low magnification in a slice of the whole retina (Fig. 4E, F). Even after photoreceptor degeneration, the ChR2-expressing RGCs remained in the ChR2V+/− rats (Fig. 4G).

When the visual signals generated by the photoreceptor cells are transmitted to inner retinal neurons, the associated change in the electric field of the retina is evaluated as the electroretinogram (ERG) response. Typical waveforms of ERGs were observed in either the ChR2V−/− or the ChR2V+/− rats (Fig. 5A; upper). We found that the a- and b-wave ERG amplitude was small in the ChR2V+/− rats when evoked by the blue LED light. Both a- and b- wave amplitudes were significantly higher in ChR2V−/− than in ChR2V+/− rats (Fig. 5B). With regard to the latency of the a-wave, no detectable difference was observed between the ChR2V−/− and ChR2V+/− rats (Fig. 5B). On the other hand, the ERG response of the ChR2V+/− rats was quantitatively similar to that of the ChR2V−/− rats when evoked by the red LED light (Fig. 5A; lower, C). Since the blue LED light, but not the red LED light, was absorbed by both the ChR2 and Venus protein, photon density of the blue LED light may have been reduced before reaching the photoreceptor cells.

After exposing the rats to 3000-lux light continuously for 7 days, the ERG responses were evaluated with the blue LED and red LED (Fig. 5D). The ERG responses were almost negligible with either the blue or the red LED at intensities of 10–1000 lux. Amplitudes of the a- or b-wave were markedly decreased in both the ChR2v −/− and +/− rats, which indicated that retinal function had been damaged by the continuous light exposure (Fig. 5E). This ERG reduction was adopted as a criterion of photoreceptor degeneration in the following experiments.

Visually Evoked Potentials

In a normal eye, the visual signal is first received by the photoreceptor cells, transmitted and integrated in the retinal neuronal network, projected to the brain by the RGCs, eventually arriving at the visual cortex through synapses in the lateral geniculate nucleus. This signaling chain is evaluated as a whole by the visually evoked potential (VEP), a visual cortical response triggered by a short light pulse. Figure 6A shows sample rat VEPs before inducing photoreceptor degeneration. VEPs were recorded in both the ChR2V−/− and ChR2V+/− rats. When the VEPs were evoked by the weak blue LED light, those of the ChR2V+/− rats were similar to those of the ChR2V−/− rats. However, with the strong blue LED light (>240 lux), the VEP of the ChR2V+/− rat was larger in amplitude and shorter in latency than that of the ChR2V−/− rat (Fig. 6B). This suggests that the strong blue LED light induces the ChR2V-expressing RGCs to fire directly, without mediation by photoreceptor cells.

On the other hand, when VEPs were evoked by the red LED light, those of the ChR2V+/− rats were similar to those of the ChR2V−/− rats in both amplitude and time course (Fig. 6A). No significant differences were present in the VEP amplitude-stimulus intensity relationships, and the latency-stimulus intensity relationship of the ChR2V+/− rats was also identical to that of the ChR2−/− rats (Fig. 6C).

The VEPs were then recorded after exposing the rats to 3000 lux light continuously for 7 days. After subsequent

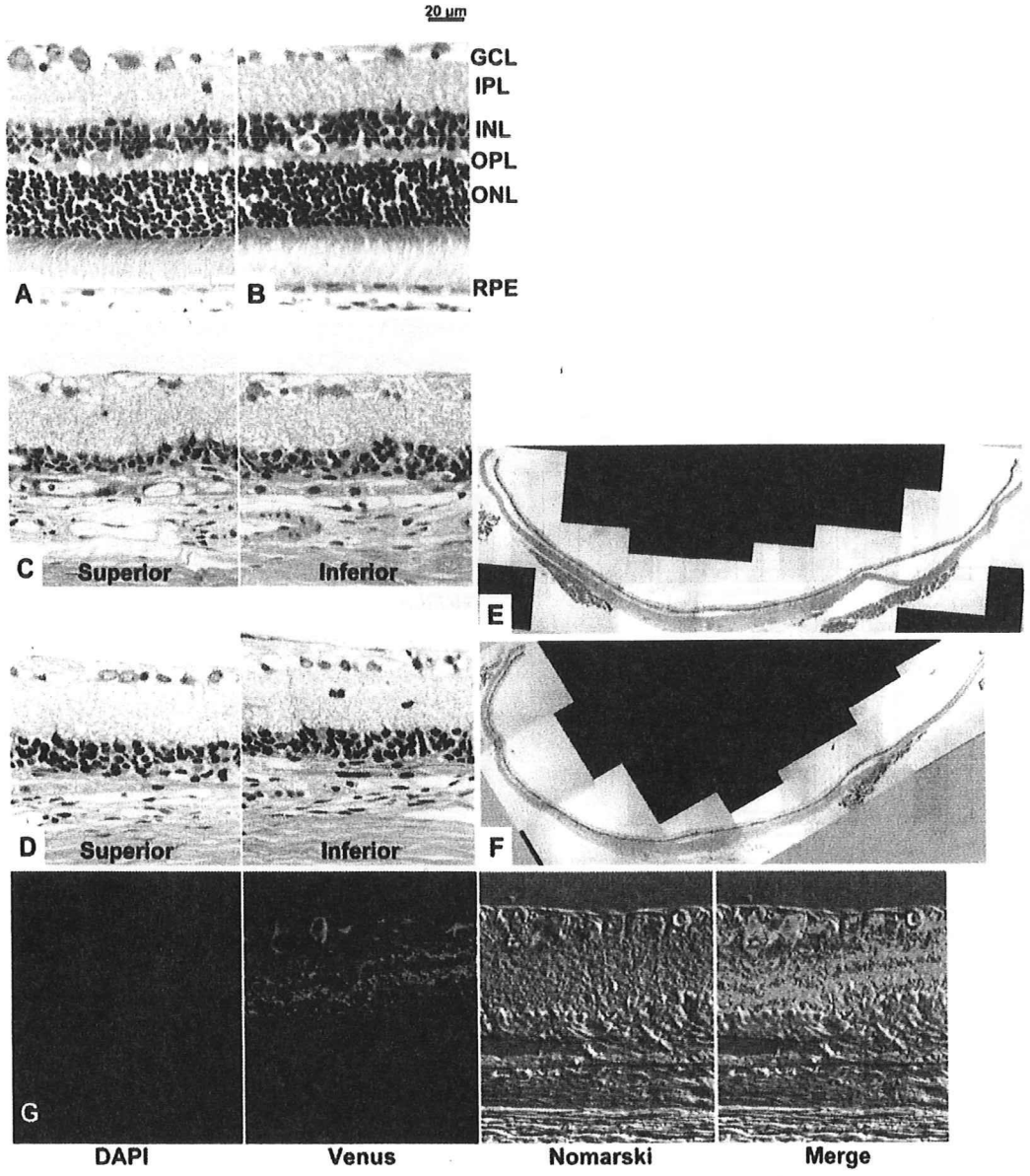

Figure 4. Morphological evidences of the photoreceptor degeneration in either ChR2V−/− or ChR2V+/− rats. (A, B) Normal retinal architecture was observed in each rat before photoreceptor degeneration. (C, D) After continuous light exposure (3000 lux for 7 days). Sections are from the superior and inferior regions at a distance of 0.24 mm from the optic nerve. Note the absence of the outer nuclear layer. (E, F)The severe degeneration extended to the whole retina. (G)Cryo-section of a retina from a ChR2V+/− rat. ChR2V expression was observed in the inner layer. Abbreviations: GCL, ganglion cell layer; IPL, inner plexiform layer; INL, inner nuclear layer; OPL, outer plexiform layer; ONL, outer nuclear layer; RPE, retinal pigment epithelium.
doi:10.1371/journal.pone.0007679.g004

degeneration of most of the photoreceptor cells, the VEPs resulting from either blue or red light were almost negligible in the ChR2V−/− rats (Fig. 7A). In contrast, in the ChR2V+/− rats, the VEPs evoked by the blue LED light clearly remained, even after photoreceptor degeneration (Fig. 7B); however, the VEPs evoked by the red LED were negligible (Fig. 7C). As shown in the amplitude-stimulus intensity relationship (Fig. 7B), the remaining VEPs were induced only by strong blue LED light (>240 lux). These VEPs were again characterized by shortened latency periods.

Optomotor Responses of the Rats

The spatial vision of an animal was quantified by its optomotor response. When a drum is rotated around an animal with printed visual stimuli on the inside wall, the animal tracks the stimulus by turning its head [23]. In our virtual optomotor system, a stimulus of blue stripes over a black background was produced according to a sine wave function with variable amplitude and frequency (Fig. 8A). With a given spatial frequency, the rat tracked the objects if the brightness-darkness contrast was high. However, the rat's response became

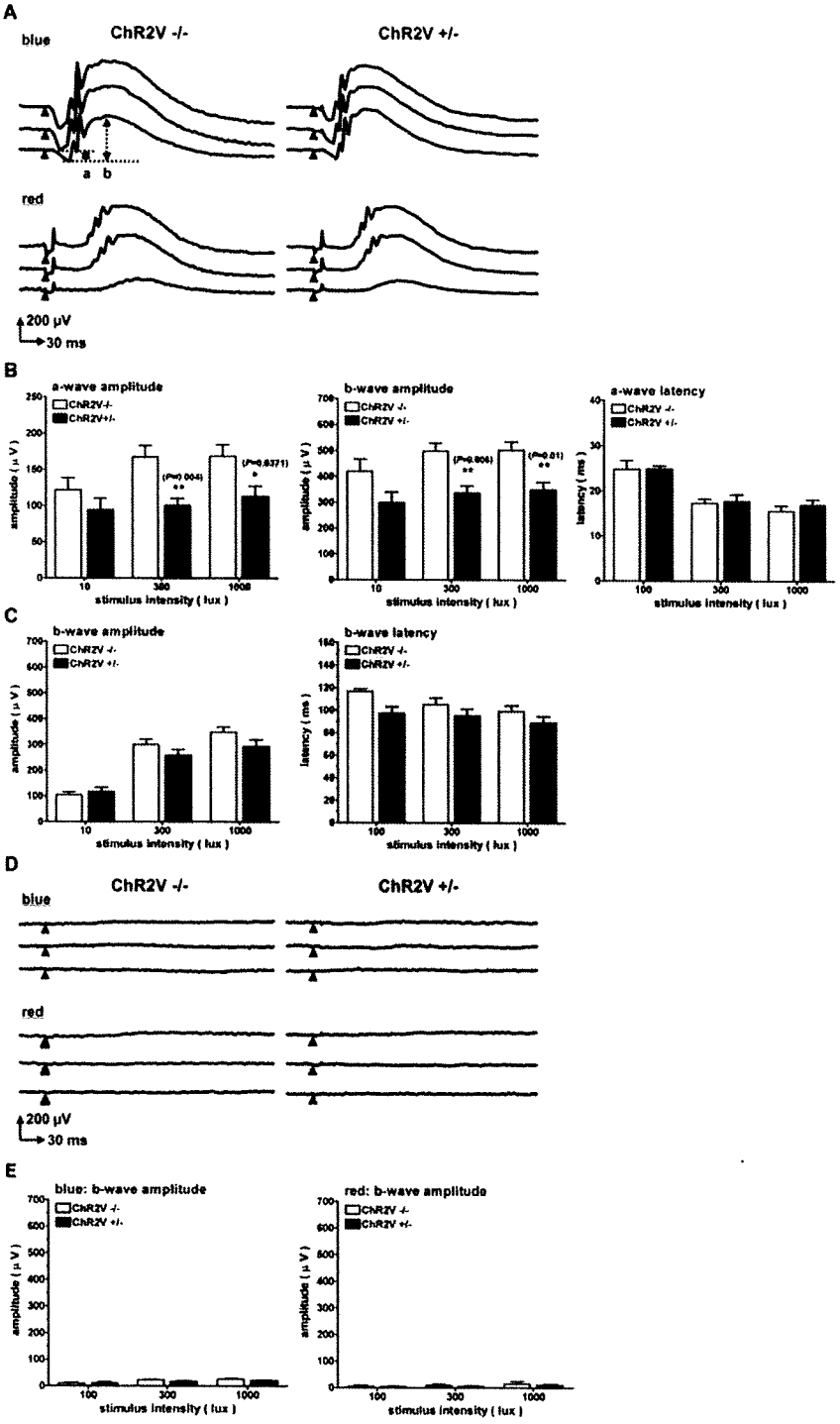

Figure 5. Electrophysiological evidence of photoreceptor degeneration. (A) Typical waveforms of electroretinogram (ERG) responses evoked by either blue or red light-emitting diode (LED) flash (duration: 10 ms; light intensity: 1000, 300, and 100 lux, top to bottom). (B)The ERG amplitudes (left, a-wave; middle, b-wave) and the latency of the a-wave (right) in response to the blue LED flash. Note that both amplitudes were significantly diminished in the ChR2V+/− rats compared to the ChR2V−/− rats without any differences in a-wave latency. (C) The b-wave amplitudes (left) and the latency (right) in response to the red LED flash. (D)Typical ERG waveforms evoked by either blue (upper traces) or red (lower traces) LED flash in the ChR2V−/− (left) and +/− (right) rats after continuous light (3000 lux) exposure for 7 days. (E)The b-wave amplitudes recorded from the rats after continuous light exposure. Error bars represent standard deviation (n = 8, **: P<0.01, unpaired t-test).
doi:10.1371/journal.pone.0007679.g005

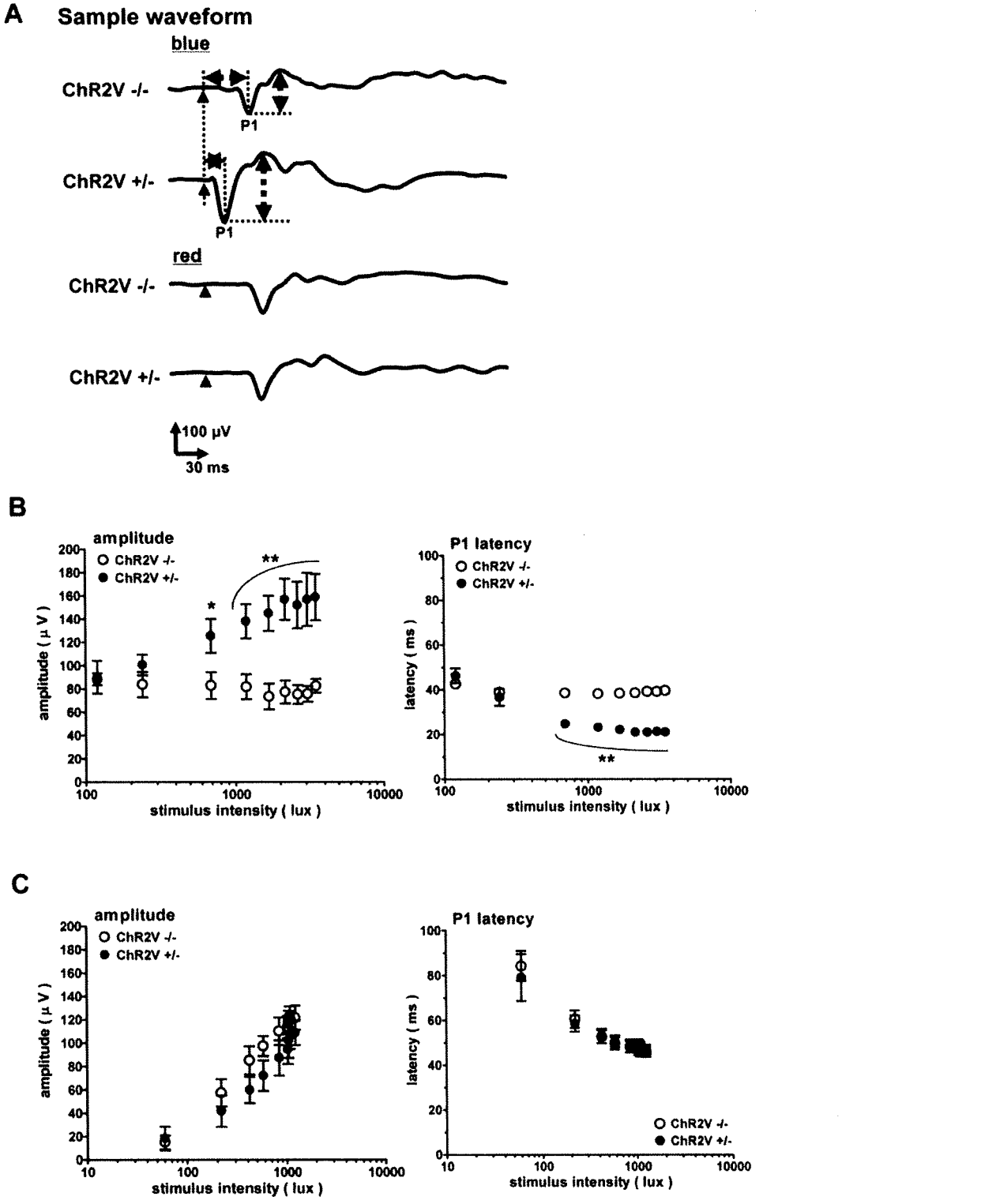

Figure 6. The visually evoked potentials recorded from either the ChR2V−/− or ChR2V+/− rats before photoreceptor degeneration. (A)Sample waveforms evoked by the blue or red LED flash. (B) The amplitude- (left) and the latency- (right) stimulus intensity relationships of VEPs evoked by the blue LED flash. (C) Similar to (A), but the responses are to the red LED flashes. Error bars represent standard deviation (n = 8, *: P = 0.04, **: P<0.01, unpaired t-test).
doi:10.1371/journal.pone.0007679.g006

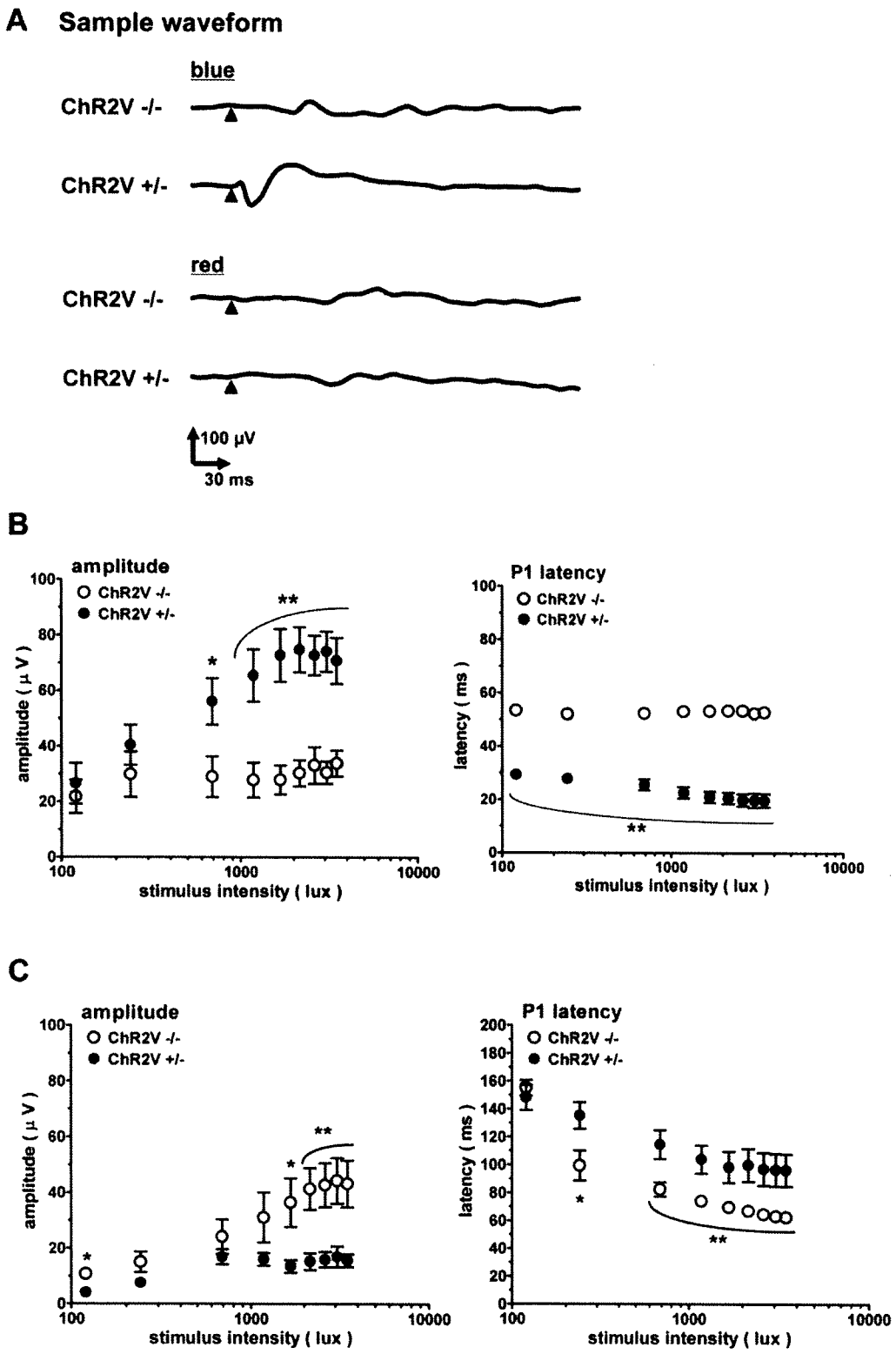

Figure 7. The VEPs after photoreceptor degeneration. (A)Sample waveforms evoked by blue or red LED flash. (B) The amplitude- (left) and the latency- (right) stimulus intensity relationships of VEPs evoked by the blue LED flash. (C) The summary of VEP responses to the red LED flashes. Error bars represent standard deviation (n=8, *: P<0.05, **: P<0.01, unpaired t-test).
doi:10.1371/journal.pone.0007679.g007

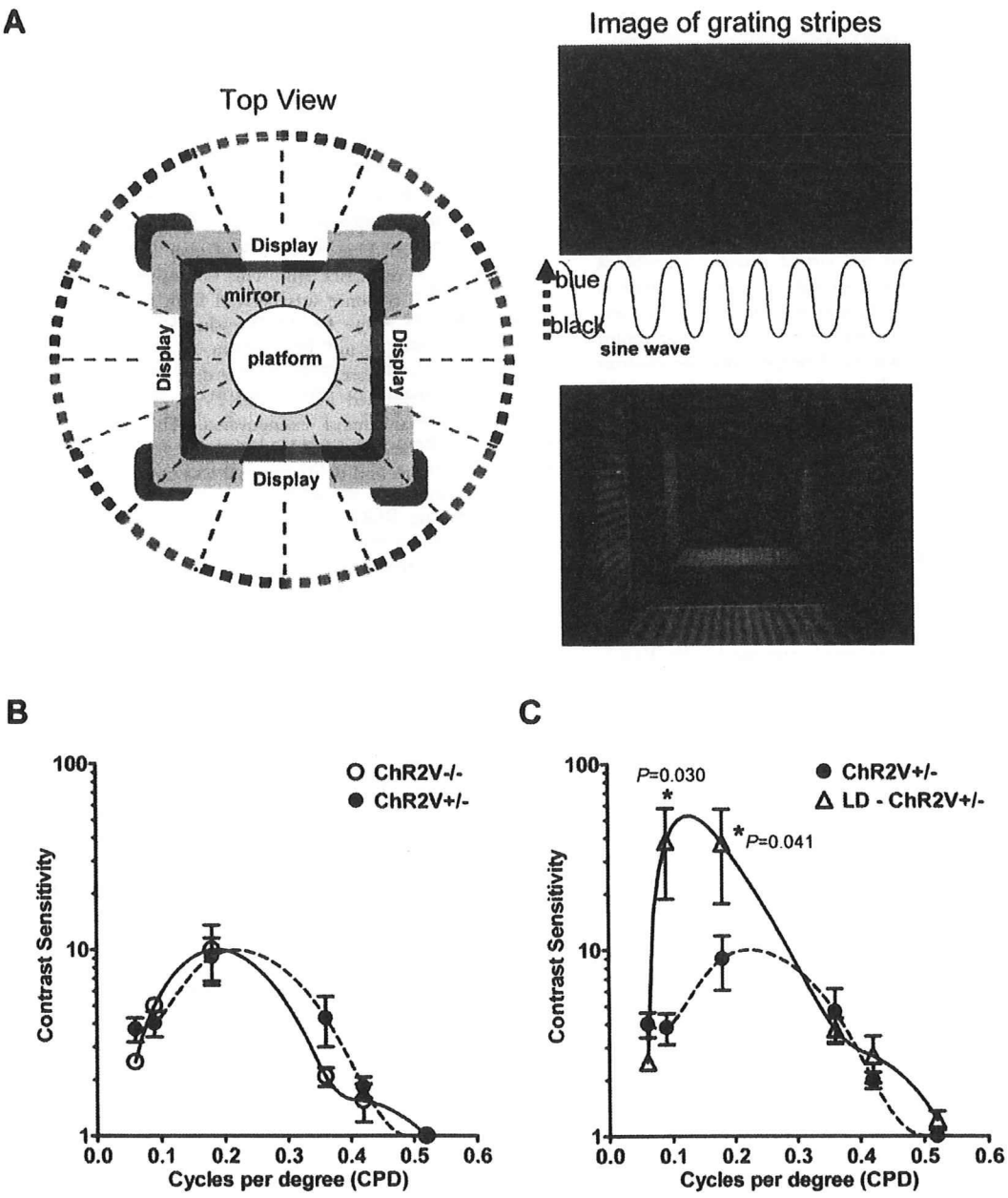

Figure 8. Optomotor response of the ChR2V−/− and ChR2V+/− rats. (A) The experimental design for the evaluation of optomotor response. The moving vertical stripes were displayed on the computer monitors so that the brightness-darkness contrast followed a sine-wave function of variable amplitude and spatial frequency. (B)The contrast sensitivity-spatial frequency relationship of the ChR2V−/− and ChR2V+/− rats before photoreceptor degeneration. (C) The contrast sensitivity-spatial frequency relationship of the ChR2V+/− rats after photoreceptor degeneration. LD = Light damaged. Error bars represent standard error of the mean (n = 8, *: P<0.05, Mann-Whitney U-test).
doi:10.1371/journal.pone.0007679.g008

undetectable when this contrast was reduced. We changed the blue/black contrast while keeping the mean brightness on the platform constant at 100 lux.

The Michelson contrast at a given spatial frequency is evaluated as follows:

$$\text{Michelson contrast} = \frac{L_{max} - L_{min}}{L_{max} + L_{min}}$$

where L_{max} is the maximal brightness (in lux) of the stimulus measured on the stage, and L_{min} is the minimal brightness (in lux). Each animal in this study tracked the virtual rotating blue/black gratings at the maximal contrast of 1. However, it stopped tracking when the contrast was reduced below a specific threshold. The reciprocal of this threshold was defined as the contrast sensitivity; once calculated, its dependence on the spatial frequency was investigated (Fig. 8B). We observed that contrast sensitivity was

small at the minimal spatial frequency of 0.06 cycles per degree (CPD), increased with the increase of spatial frequency, reached a maximum around 0.18 CPD, and was negligible at spatial frequencies over 0.52 CPD. Therefore, the relationship followed an inverted U-shaped curve, as noted in previous reports [23,24]. We found that the optomotor responses of the ChR2V+/− rats were similar to those of the ChR2V−/− rats with regard to the contrast sensitivity-spatial frequency relationship.

The optomotor response of ChR2V−/− rats was severely reduced after exposing the rats to 3000-lux light continuously for 7 days. They no longer tracked the virtual rotating blue/black gratings at any spatial frequency, even with a maximal contrast of 1. In the ChR2V+/− rats, no reduction of contrast sensitivity was observed at any spatial frequency, even after photoreceptor degeneration (Fig. 8C and Movie S1). Unexpectedly, the contrast sensitivity was instead somewhat enhanced at a low spatial frequency such as 0.09 or 0.18 CPD.

Discussion

In the present paper, we tested the possibility that RGCs can behave as photoreceptor cells when they are endowed with photosensitivity. We investigated this by using a line of transgenic rats, W-TChR2V4, in which the ChR2 gene was expressed selectively in RGCs under the regulation of the Thy-1.2 promoter. In heterozygous rats where ChR2 was conjugated with a fluorescent marker, ChR2 was exclusively expressed in the RGCs. Stimulation with blue LED light directly evoked action potentials in the ChR2V-expressing RGCs. The VEP in transgenic rats with intact photoreceptors consisted of two components with either a short or a long latency. The short-latency component appeared to be derived from the direct photosensitive response of the RGCs, whereas the long-latency component was dependent on the retinal rod photoreceptor cells. The head-tracking behavior of the ChR2V+/− rats showed that they followed the virtual rotation of light-dark gratings even after the massive degeneration of photoreceptor cells. This evidence suggests that ChR2-expressing RGCs are substitutable for rod photoreceptor cells in the retina.

Selective Expression of ChR2 in the RGCs

In the present study, we established several lines of transgenic rats in which ChR2 expression was driven by the Thy-1.2 promoter. The phenotypic expression of ChR2 was detected in the retina by the coexpression of the fluorescent protein "Venus," which is connected at the C-terminal end of the N-terminal 315 amino acid fragment of ChR2. We found that phenotypic expression varied from line to line. In some lines such as W-TChR2V1, W-TChR2V5, and W-TChR2V6, ChR2 was expressed in nonganglion cells such as amacrine, bipolar, and Müller. This is consistent with findings that the Thy-1.2 antigen is expressed in some of these cells at low level, even though Thy-1.2 has been considered to be a "specific" marker of RCGs [16,17,25]. Feng et al. [26] observed various GFP expression patterns among transgenic mouse lines in which GFP expression was driven by the Thy-1.2 gene. This variation may reflect differences in integration sites in the chromosomes and/or the number of inserted copies. One of our lines, W-TChR2V4, expressed ChR2 nearly selectively in RGCs. Therefore, this line appeared to be the most suitable line for studying visual function produced by ChR2-transferred RGCs. When the RGCs of this line were retrogradely labeled with a fluorogold applied to the superior colliculus, 45.7%±8.4% of the fluorogold-positive RGCs were also expressing ChR2V. It is possible that ChR2V-positive and −negative RGCs have different morphological and/or physiological traits [10,11,27,28,29,30], although further experiments are necessary to reveal such correlations.

Visual Responses Dependent on the ChR2-Expressing RCGs

One of our novel findings was the presence of an early VEP component in the ChR2V+/− rats. The mean latency of this component was 20 ms, suggesting that no more than one synapse was involved in the pathway. The early VEP component was only evoked by bright blue LED light of over 240 lux, but was not evoked by the red LED light. This is consistent with the notion that this VEP response was derived from the direct and rapid depolarization of the ChR2-expressing RGCs, since ChR2 is exclusively sensitive to the blue light, with a peak sensitivity at 460–480 nm [5]. After photoreceptor degeneration, the early VEP component remained in the ChR2V+/− rats, while the late component was almost extinguished. This evidence strongly suggests that the blue LED light directly evoked action potentials in these neurons and that the signal was conducted to the visual cortex via synapses in the lateral geniculate nucleus. That is, the ChR2-expressing RGCs acted as extra photoreceptors in these animals. Thus, the visual cortex accepted the signals derived from these photosensitive RGCs in parallel with those derived from retinal photoreceptor cells. Previously, we reported that the VEP was restored when the ChR2 gene was delivered to the retinal cells in aged dystrophic Royal College of Surgeons (RCS) rats in which the photoreceptor cells were degenerated [9]. Re-evaluation of this VEP latency revealed that it was approximately 20 ms. This was smaller than the latency of the VEP evoked in nondystrophic RCS rats without ChR2 gene induction.

We also investigated the optomotor response of the ChR2V+/− rats using virtual rotating blue/black gratings. The head-tracking behavior with contrast sensitivity in these animals was no less than that of the ChR2V−/− rats. Thus, the signals from the ChR2-expressing RGCs appear not to have interfered with those derived from the photoreceptor cells. Therefore, it is possible that these signals are integrated in the visual cortex to produce appropriate vision.

Visual Responses after Photoreceptor Degeneration

To explore the visual function produced by ChR2-expressing RGCs, we induced the degeneration of native photoreceptor cells using the light-induced photoreceptor degeneration model [31], which is commonly used to study the mechanisms of stress-induced photoreceptor degeneration [32,33,34]. In this animal model as well as in inherited retinal degeneration, the "final common pathway" of photoreceptor cell death is considered to be apoptosis [35,36] although cones in retinal degeneration (RD), even if they loose their function, can survive for very long time, i.e. cone apoptosis does not occur necessarily in some RD patients [37]. In the present study, rats were exposed to 3000 lux light continuously for 7 days so that photoreceptor cells were not protected by the mechanisms underlying bright cyclic light rearing [38,39,40]. When the retinas of the light-exposed animals were histologically examined, the photoreceptor cells had almost disappeared. The ERG responses were almost entirely extinguished in the present study; therefore, the native photoreceptor activity was clearly diminished by the continuous light exposure.

Even in the absence of photoreceptor cell activity, the visual cortex of the ChR2V+/− rats received visual signals derived from the ChR2-expressing RGCs, as evidenced by the remaining early VEP component. Are these signals correctly interpreted by the brain to form behavior-related vision? In the present study, we investigated the optomotor response of the ChR2V+/− rats after

continuous light exposure. These animals did indeed track the virtual rotating blue/black gratings with contrast sensitivity no less than before photoreceptor degeneration. Thus, we suggest that the visual signals derived from the ChR2-expressing RGCs are reinterpreted by the brain as some form of vision.

Nevertheless, these animals did appear to sense their environment differently from the controls. For example, they were only sensitive to bright blue light. With this light stimulus, they showed enhanced contrast sensitivity to the virtual rotating gratings at low spatial frequency. It is possible that the visual signals derived from the ChR2-expressing RGCs are particularly suitable to this kind of visual information. On the other hand, the visual signals derived from the native photoreceptor cells appear to be adapted to a broader range of spatial frequencies. Although these two pathways may possibly raise a visual rivalry in the visual system, the pathway driven by the photoreceptor cell activation may overcome the pathway driven by activation of the ChR2-expressing RGC. Further studies are necessary to evaluate this possibility.

In conclusion, we created a model transgenic rat system and demonstrated that RGCs behave as additional photoreceptor cells if they are expressing ChR2. Since RGCs are preserved in the retina of patients with photoreceptor degeneration, such as that occurring in retinitis pigmentosa, the delivery of the ChR2 gene would restore patients' vision to some extent. Since RGCs are physiologically heterogeneous [28,41], it would be ideal if ChR2 were expressed exclusively in the ON-type RGCs for improvement of vision. Our study revealed that the visual signals derived from the ChR2-expressing RGCs are reinterpreted by the brain to form a kind of vision, even if the expression is nonselective.

Materials and Methods

Animals

All experiments were conducted with the approval of the Animal Research Committee, Graduate School of Medicine, Tohoku University and the National Institute for Physiological Science's Animal Care and Use Committee. Rats were kept in cyclic light (12 hours ON/OFF: 200 lux/dark) after birth and fed laboratory chow *ad libitum* with free access to water.

Generation of Transgenic Rats

We followed the protocol previously described by Feng et al. [26] to generate Thy-1.2 transgenic rats. The Thy-1.2 vector was generously provided to us by Dr. Joshua Sanes (Washington University, Saint Louis, MO) and has been described by Vidal et al. [42], Kelley et al. [43], and Caroni et al. [21] (Fig. 1A). The Thy-1.2 vector contained 6.5 kb of the murine Thy-1.2 gene extending from the promoter to the intron following exon 4, without exon 3 and the flanking introns [21]. The targeting vector was constructed by inserting a DNA fragment coding the ChR2 (a generous gift from Dr. G. Nagel, Universität Würzberg, Würzberg, Germany) fused to the Venus gene (a generous gift from Dr. A. Miyawaki, RIKEN BSI, Wako-shi, Japan) into the XhoI site of the Thy-1.2 vector (Thy-1.2-ChR2V; Fig. 1A). A 8.1-kbp of Thy-1.2 ChR2V DNA solution at a concentration of 5 μg/ml was microinjected into pronuclear-stage zygotes of Wistar rats to produce transgenic rats [44]. Transgenic founders were crossed for one to four generations before initiating a detailed analysis of expression patterns.

Screenings of Transgenic Line

Rats were screened by genomic PCR for the presence of the transgene. Genomic DNA was isolated by incubating rat tail (−3 mm) in 500 μl of tail lysis buffer (100 mM Tris-HCl [pH 8.0], 5 mM EDTA [pH 8.0], 200 mM NaCl, 0.2% [w/v] SDS, and proteinase K 100 μg/ml) overnight at 55°C. The mixture was shaken vigorously and centrifuged at 12000 rpm for 10 min at room temperature. Five hundred μl of isopropanol was added to the supernatant, and the contents mixed by inversion. The stringy precipitate of DNA was transferred to a new tube with a clean glass capillary. The DNA was dissolved in 300 μl of TE (pH 8.0). The forward primer (5′-TCTGAGTGGCAAAGGACCTTAGG-3′) and reverse primer (5′-CGCTGAACTTGTGGCCGTT-TACG-3′) for the cDNA sequence of fluorescent protein were used at an annealing temperature of 62°C. A primer pair for the T cell receptor gene (5′-CAAATGTTGCTTGTCTGTG-3′ as a forward primer and 5′-GTCAGTCGAGTGCACAGTTT-3′ as a reverse primer) was used for positive control of the genomic DNA. For the examination of the expression of ChR2-Venus in the retina, a few rats of each positive line were perfused with a fixative solution containing 4% paraformaldehyde and 15% saturated picric acid in 0.1 M phosphate buffer (pH 7.2) under deep anesthesia. Eyes were removed and fixed further with 4% paraformaldehyde in 0.1 M phosphate buffered saline (PBS) overnight at 4°C. The flat-mounted retina was made with one of the pair of eyes. The contralateral eyes were embedded in optimal cutting temperature (OCT) compound (Sakura, Tokyo, Japan) following immersion in 30% sucrose solution with PBS. Ten-micrometer retinal sections were made and mounted on slides. The flat-mounted retinas and sections were covered with Vectashield medium (Vector Laboratories, Burlingame, CA). For staining of nuclei with DAPI, retinal slices were covered with Vectashield medium including DAPI (Vector Laboratories). Venus fluorescence was visualized under the Axiovert40 fluorescence microscope (Carl Zeiss).

Maintenance of Transgenic Rat Lines

Transgenic lines were maintained by cross breeding for more than four generations with the genetic background of Wistar rats. Littermates were screened by genomic PCR using the primers indicated above. Two-month-old littermates were divided to two groups as negative (ChR2V−/−) and positive (ChR2V+/−) for the induction of photoreceptor degeneration.

Retrograde Labeling of RGCs with a Fluorescent Tracer, Fluorogold

To identify RGCs in the ganglion cell layer (GCL), retrograde labeling was performed 7 days before the rats were sacrificed. The labeling was done by injecting 4 μl of 2% aqueous fluorogold (FG; Fluorochrome, Englewood, CO) [45] containing 1% dimethyl sulfoxide (DMSO) into the superior colliculus using a Hamilton syringe with a 32 G needle [46].

Induction of Photoreceptor Degeneration

To induce severe photoreceptor degeneration, the conditions under which the rats were kept was changed to cyclic light (12 hours ON/OFF: 5–10 lux/dark) at least 2 weeks before the light exposure. Rats were then exposed to 3000-lux intensity of fluorescent light for 7 days. We used a light exposure box (NK Systems, Tokyo, Japan) to control the timing and light intensity for the induction of photoreceptor degeneration.

Histological Studies of Retina

Analysis of retinal morphologies in ChR2V−/− and ChR2V+/− rats were performed as previously described by Li et al [32]. In brief, rats were sacrificed by asphyxiation with carbon dioxide after the induction of photoreceptor degeneration. The

eyes were enucleated, fixed, and embedded in paraffin. Three-micrometer thick sections of retinas were cut along the vertical meridian and stained with hematoxylin and eosin to allow examination of the retina in the superior and inferior hemispheres [47].

Electrophysiology of RGCs

Rats were ether-anesthetized, and both left and right eyes were quickly removed and dissected in a cutting solution containing (in mM) 229 mannitol, 3 KCl, 26 $NaHCO_3$, 1 H_3PO_4, and 7 $MgCl_2$, pH 7.4 (4°C) equilibrated with 95% O_2 and 5% CO_2 mixed gas. The retina was removed from the pigment epithelium, vitreous side up, and superfused by an artificial cerebrospinal fluid (ACSF) containing (in mM) 114 NaCl, 2.5 KCl, 26 $NaHCO_3$, 1 NaH_2PO_4, 10 mannitol, 2.5 $CaCl_2$, 1.3 $MgCl_2$, and 10 glucose (pH 7.4 with 95% O_2 and 5% CO_2 mixed gas). To block the photoreceptor-derived inputs, kynurenic acid (1 mM, Sigma-Aldrich) was included in the solutions throughout the experiments. Whole-cell patch-clamp recordings were made from ChR2V-expressing cells visually identified under conventional epifluorescent microscopy (BX50WI, Olympus) equipped with a 60× water objective lens (LUMplanPl/IR60×, Olympus), using a conventional patch clamp system (EPC-7 plus, HEKA and Digidata 1440A, Molecular Devices Co., Sunnyvale, CA). The patch pipette solution contained (in mM): 120 KOH, 100 glutamic acid, 5 HEPES, 2.5 $MgCl_2$, 2.5 MgATP, 5 Na_2EGTA, 1.2 leupeptin (pH 7.4 by KOH). In some experiments, 1% dextran tetramethylrhodamine (Molecular Probes, Eugene, OR, USA) was included to facilitate identification of the recorded cell. Liquid junction potentials were not corrected. After establishing a tight seal, the optical filter set was changed to one equipped with a blue LED (470±25 nm wavelength, LXHL-NB98, Lumileds Lighting Inc., San Jose, CA). Pulsed light was emitted by applying square electrical pulses of 1.5–2.0 V. The light power density was directly measured by a thermopile (MIR-100Q, Mitsubishi Oil Chemicals, Tokyo, Japan). All the experiments were carried out at 27–30°C.

Recording of ERGs and VEPs

ERGs and VEPs were recorded using a Neuropack (MEB-9102; Nihon Kohden, Tokyo, Japan) according to the methods previously described by Tomita et al. [9]. Briefly, rats were dark-adapted overnight, the pupils were dilated with 1% atropine and 2.5% phenylephrine hydrochloride, and the corneas were anaesthetized with 0.5% propacaine hydrochloride. Small contact lenses with gold wire loops were placed on both corneas, and a silver wire reference electrode was placed subcutaneously between the eyes. Flash light stimuli of 10 ms duration were generated by pulse activation of a blue or white LED. Full-field scotopic ERGs were recorded, band-pass filtered at 0.3–500 Hz, and averaged for five responses at each light intensity. The amplitude of the a- and b-wave was measured when both were clearly detected. For recording VEPs, recording electrodes (silver-silver chloride) were placed epidurally on each side 7 mm behind the bregma and 3 mm lateral of the midline, and a reference electrode was placed epidurally on the midline 12 mm behind the bregma at least 7 days before the experiments. Under ketamine-xylazine anesthesia, the pupils were dilated with 1% atropine and 2.5% phenylephrine hydrochloride. The ground electrode clip was placed on the tail. Photic stimuli of 20-ms duration under various intensities were applied with a frequency of 0.5 Hz. Photic stimuli were generated by pulse activation of a blue LED with light emitting wavelengths of 435–500 nm (peak at 470 nm) or a red LED (580–640 nm, peak at 625 nm). The high and low pass filters were set to 50 kHz and 0.05 kHz, respectively. One hundred consecutive response waveforms were averaged for each VEP measurement.

Behavioral Tests

We used a virtual optomotor system to evaluate the optomotor responses. The original virtual optomotor system described by Prusky et al. [23] was modified for rats. A light-dark grating pattern was displayed on computer monitors (ProLite E1902WS; Iiyama, Tokyo, Japan) arranged in a square around a platform. A video camera was stationed 50 cm above the platform. The grating patterns, which were determined by a sine wave function with variable spatial frequency and contrast, were produced by a program we developed using the Visual Basic 2007 programming language (Microsoft). The software also controlled the speed of virtual optomotor rotation, which was set at 12 degrees per second (2 rpm) in all experiments. The spatial frequency and the contrast of the grating pattern was varied but the average brightness kept constant. The illuminance at the center of the platform was 200, 100, and 0.5 lux when the color was set to white, blue, or black, respectively. Mirrors covered the platform above and below. From the perspective of the rat, the environment was like a 3-D world surrounded by moving light-dark vertical gratings.

The animal was allowed to move freely on the platform in the virtual optomotor system. The experimenter waited until it stopped moving, and then a homogeneous gray stimulus was projected for 30 s on the monitors before the presentation of each grating session, which was also timed for 30 s. The grating session was started from a low spatial frequency (0.06 cycles/degree) with the maximal contrast. An experimenter assessed whether the animals tracked the rotation by monitoring the head movement and the presented rotating stimulus simultaneously on another display connected to the video camera. If head movement simultaneous with the rotation was evident, the experimenter judged that the animal could discriminate the grating and proceeded to the next grating session. If the movement was ambiguous, the same grating session was presented again. All behavioral tests were double blind and performed during the first few hours of the animals' light cycle (light on at 8 AM).

Statistical Analysis

Statistical analysis was performed using GraphPad Prism software (GraphPad Software, San Diego, CA). The criterion for statistical significance was $P<0.05$. The statistical methods used were the unpaired t-test and the Mann-Whitney U-test for the electrophysiological studies and the behavioral studies, respectively.

Supporting Information

Movie S1 The movie of optomotor response in photoreceptor degenerated ChR2V+/− rat. The ChR2V+/− rat was exposed to 3000-lux intensity of fluorescent light for 7 days to induce photoreceptor degeneration. The responses of ERGs were negligible by either blue or red light (Fig. 7A). The head-tracking behavior was evaluated using a virtual optomotor system. Three digits showed the spatial frequency (cycles per degree) under the left.

Found at: doi:10.1371/journal.pone.0007679.s001 (2.90 MB MPG)

Author Contributions

Conceived and designed the experiments: HT ES YF TI RS. Performed the experiments: HT ES YF HI YS TH MK MH. Analyzed the data: HT. Contributed reagents/materials/analysis tools: HM. Wrote the paper: HT HY MT.

References

1. Hartong DT, Berson EL, Dryja TP (2006) Retinitis pigmentosa. Lancet 368: 1795–1809.
2. Humayun MS, Prince M, de Juan E, Jr., Barron Y, Moskowitz M, et al. (1999) Morphometric analysis of the extramacular retina from postmortem eyes with retinitis pigmentosa. Invest Ophthalmol Vis Sci 40: 143–148.
3. Santos A, Humayun MS, de Juan E, Jr., Greenburg RJ, Marsh MJ, et al. (1997) Preservation of the inner retina in retinitis pigmentosa. A morphometric analysis. Arch Ophthalmol 115: 511–515.
4. Stone JL, Barlow WE, Humayun MS, de Juan E, Jr., Milam AH (1992) Morphometric analysis of macular photoreceptors and ganglion cells in retinas with retinitis pigmentosa. Arch Ophthalmol 110: 1634–1639.
5. Nagel G, Szellas T, Huhn W, Kateriya S, Adeishvili N, et al. (2003) Channelrhodopsin-2, a directly light-gated cation-selective membrane channel. Proc Natl Acad Sci U S A 100: 13940–13945.
6. Ishizuka T, Kakuda M, Araki R, Yawo H (2006) Kinetic evaluation of photosensitivity in genetically engineered neurons expressing green algae light-gated channels. Neurosci Res 54: 85–94.
7. Nagel G, Brauner M, Liewald JF, Adeishvili N, Bamberg E, et al. (2005) Light activation of channelrhodopsin-2 in excitable cells of Caenorhabditis elegans triggers rapid behavioral responses. Curr Biol 15: 2279–2284.
8. Bi A, Cui J, Ma YP, Olshevskaya E, Pu M, et al. (2006) Ectopic expression of a microbial-type rhodopsin restores visual responses in mice with photoreceptor degeneration. Neuron 50: 23–33.
9. Tomita H, Sugano E, Yawo H, Ishizuka T, Isago H, et al. (2007) Restoration of visual response in aged dystrophic RCS rats using AAV-mediated channelopsin-2 gene transfer. Invest Ophthalmol Vis Sci 48: 3821–3826.
10. Dowling JE (1999) Retinal processing of visual information. Brain Res Bull 50: 317.
11. Kuffler SW (1953) Discharge patterns and functional organization of mammalian retina. J Neurophysiol 16: 37–68.
12. Morris RJ, Williams AF (1977) Serological and preliminary biochemical characteristics of a T lymphocyte differentiation antigen detected by rabbit antiserum to rat thymocyte membranes. Eur J Immunol 7: 360–366.
13. Fields KL, Brockes JP, Mirsky R, Wendon LM (1978) Cell surface markers for distinguishing different types of rat dorsal root ganglion cells in culture. Cell 14: 43–51.
14. Barclay AN, Hyden H (1978) Localizatin of the Thy-1 antigen in rat brain and spinal cord by immunofluorescence. J Neurochem 31: 1375–1391.
15. Mason DW, Williams AF (1980) The kinetics of antibody binding to membrane antigens in solution and at the cell surface. Biochem J 187: 1–20.
16. Perry VH, Morris RJ, Raisman G (1984) Is Thy-1 expressed only by ganglion cells and their axons in the retina and optic nerve? J Neurocytol 13: 809–824.
17. Barnstable CJ, Drager UC (1984) Thy-1 antigen: a ganglion cell specific marker in rodent retina. Neuroscience 11: 847–855.
18. Hayworth CR, Rojas JC, Gonzalez-Lima F (2008) Transgenic mice expressing cyan fluorescent protein as a reporter strain to detect the effects of rotenone toxicity on retinal ganglion cells. J Toxicol Environ Health A 71: 1582–1592.
19. Kerrison JB, Duh EJ, Yu Y, Otteson DC, Zack DJ (2005) A system for inducible gene expression in retinal ganglion cells. Invest Ophthalmol Vis Sci 46: 2932–2939.
20. Leung CK, Lindsey JD, Crowston JG, Ju WK, Liu Q, et al. (2008) In vivo imaging of murine retinal ganglion cells. J Neurosci Methods 168: 475–478.
21. Caroni P (1997) Overexpression of growth-associated proteins in the neurons of adult transgenic mice. J Neurosci Methods 71: 3–9.
22. Rapp LM, Smith SC (1992) Morphologic comparisons between rhodopsin-mediated and short-wavelength classes of retinal light damage. Invest Ophthalmol Vis Sci 33: 3367–3377.
23. Prusky GT, Alam NM, Beekman S, Douglas RM (2004) Rapid quantification of adult and developing mouse spatial vision using a virtual optomotor system. Invest Ophthalmol Vis Sci 45: 4611–4616.
24. McGill TJ, Douglas RM, Lund RD, Prusky GT (2004) Quantification of spatial vision in the Royal College of Surgeons rat. Invest Ophthalmol Vis Sci 45: 932–936.
25. Dabin I, Barnstable CJ (1995) Rat retinal Muller cells express Thy-1 following neuronal cell death. Glia 14: 23–32.
26. Feng G, Mellor RH, Bernstein M, Keller-Peck C, Nguyen QT, et al. (2000) Imaging neuronal subsets in transgenic mice expressing multiple spectral variants of GFP. Neuron 28: 41–51.
27. Huxlin KR, Goodchild AK (1997) Retinal ganglion cells in the albino rat: revised morphological classification. J Comp Neurol 385: 309–323.
28. Masland RH (2001) The fundamental plan of the retina. Nat Neurosci 4: 877–886.
29. Rockhill RL, Daly FJ, MacNeil MA, Brown SP, Masland RH (2002) The diversity of ganglion cells in a mammalian retina. J Neurosci 22: 3831–3843.
30. Yin L, Smith RG, Sterling P, Brainard DH (2009) Physiology and morphology of color-opponent ganglion cells in a retina expressing a dual gradient of S and M opsins. J Neurosci 29: 2706–2724.
31. Noell WK, Walker VS, Kang BS, Berman S (1966) Retinal damage by light in rats. Invest Ophthalmol 5: 450–473.
32. Li G, Anderson RE, Tomita H, Adler R, Liu X, et al. (2007) Nonredundant role of Akt2 for neuroprotection of rod photoreceptor cells from light-induced cell death. J Neurosci 27: 203–211.
33. Sugano E, Tomita H, Ishiguro S, Abe T, Tamai M (2005) Establishment of effective methods for transducing genes into iris pigment epithelial cells by using adeno-associated virus type 2. Invest Ophthalmol Vis Sci 46: 3341–3348.
34. Tomita H, Kotake Y, Anderson RE (2005) Mechanism of protection from light-induced retinal degeneration by the synthetic antioxidant phenyl-N-tert-butylnitrone. Invest Ophthalmol Vis Sci 46: 427–434.
35. Hafezi F, Marti A, Munz K, Reme CE (1997) Light-induced apoptosis: differential timing in the retina and pigment epithelium. Exp Eye Res 64: 963–970.
36. Reme CE, Grimm C, Hafezi F, Marti A, Wenzel A (1998) Apoptotic cell death in retinal degenerations. Prog Retin Eye Res 17: 443–464.
37. Lin B, Masland RH, Strettoi E (2009) Remodeling of cone photoreceptor cells after rod degeneration in rd mice. Exp Eye Res 88: 589–599.
38. Huang H, Frank MB, Dozmorov I, Cao W, Cadwell C, et al. (2005) Identification of mouse retinal genes differentially regulated by dim and bright cyclic light rearing. Exp Eye Res 80: 727–739.
39. Kaldi I, Martin RE, Huang H, Brush RS, Morrison KA, et al. (2003) Bright cyclic rearing protects albino mouse retina against acute light-induced apoptosis. Mol Vis 9: 337–344.
40. Li F, Cao W, Anderson RE (2001) Protection of photoreceptor cells in adult rats from light-induced degeneration by adaptation to bright cyclic light. Exp Eye Res 73: 569–577.
41. Masland RH (2001) Neuronal diversity in the retina. Curr Opin Neurobiol 11: 431–436.
42. Vidal M, Morris R, Grosveld F, Spanopoulou E (1990) Tissue-specific control elements of the Thy-1 gene. Embo J 9: 833–840.
43. Kelley KA, Friedrich VL, Jr., Sonshine A, Hu Y, Lax J, et al. (1994) Expression of Thy-1/lacZ fusion genes in the CNS of transgenic mice. Brain Res Mol Brain Res 24: 261–274.
44. Takahashi R, Hirabayashi M, Ueda M (1999) Production of transgenic rats using cryopreserved pronuclear-stage zygotes. Transgenic Res 8: 397–400.
45. Brecha NC, Weigmann C (1994) Expression of GAT-1, a high-affinity gamma-aminobutyric acid plasma membrane transporter in the rat retina. J Comp Neurol 345: 602–611.
46. Sato H, Tomita H, Nakazawa T, Wakana S, Tamai M (2005) Deleted in polyposis 1-like 1 gene (Dp111): a novel gene richly expressed in retinal ganglion cells. Invest Ophthalmol Vis Sci 46: 791–796.
47. LaVail MM, Unoki K, Yasumura D, Matthes MT, Yancopoulos GD, et al. (1992) Multiple growth factors, cytokines, and neurotrophins rescue photoreceptors from the damaging effects of constant light. Proc Natl Acad Sci U S A 89: 11249–11253.

—Mini Review—

Morphological Evaluation and Measurement of the Respiration Activity of Cumulus-oocyte Complexes to Assess Oocyte Quality

Haruo Murakawa[1]*, Nobuya Aono[1], Takayuki Tanaka[1], Hiroyuki Kikuchi[1], Hidemune Yoshida[1], Hiroaki Yoshida[1], Masaki Yokoo[2] and Hiroyuki Abe[3]

[1]Reproductive Research Center, Yoshida Ladies Clinic, Sendai 981-1105, Japan
[2]Innovation of New Biomedical Engineering Center, Tohoku University, Sendai 980-8574, Japan
[3]Graduate School of Science and Engineering, Yamagata University, Yonezawa 992-8510, Japan

Abstract: Scanning electrochemical microscopy (SECM) is a non-invasive and sensitive technique for measuring cellular respiration. In this paper, we review the SECM technique, to establish it as an accurate method for measuring the respiratory activity of single cumulus-oocyte complexes (COCs) and oocytes in animals as well as in humans. Oxygen consumption rates of COCs are influenced by the surrounding cumulus volume and the mitochondrial activity of the cumulus cells. An increase in the oxygen consumption rate was found in bovine oocytes, whereas the oxygen consumption of human oocytes tends to decrease during in vitro maturation (IVM). To analyze the metabolic activity of mitochondrial respiration, ATP content and mitochondrial distribution in bovine oocytes have been examined. An electron microscopic study confirmed mitochondrial reorganization in bovine oocytes during oocyte maturation. These results show that the respiratory activity of oocytes changes with maturation status during IVM and mitochondrial reorganization may partly influence respiratory activity. The SECM procedure is therefore a useful technique for evaluating the metabolic activity and quality of oocytes and cumulus cells in the IVM process.

Key words: Cumulus cells, Oocyte maturation, Mitochondria, Oxygen consumption, Electrochemical measurement

Received: January 7, 2009
Accepted: February 26, 2009
*To whom correspondence should be addressed.
e-mail: repro@yoshida-lc.jp

Introduction

The *in vitro* maturation (IVM) of human oocytes is an attractive technique that provides a patient-friendly approach to assisted reproductive technology. IVM is relatively simple with a shorter period of treatment and lower costs than conventional *in vivo* fertilization (IVF). For anovulatory patients with polycystic ovaries (PCO), a decrease in the dose of ovarian stimulating drugs lowers the risk of ovarian hyperstimulation syndrome. IVM has been successfully applied to animals [1, 2]. Cha *et al.* were the first group to show the success of IVM in human beings using immature donor oocytes retrieved from antral follicles [3]. Recent studies have demonstrated that the results from IVM are comparable to those achieved with contemporary IVF [4, 5]. The applicability and development of IVM technology is dependent on the improvement of *in vitro* culture systems. During *in vitro* culture, cumulus cells play an important role in oocyte maturation. If provided with the several factors that are essential for normal nuclear and cytoplasmic maturation, oocytes can mature and develop to an embryo after fertilization [6]. Therefore, an appropriate evaluation of cumulus-oocyte complexes (COCs) is indispensable for evaluating the quality of oocytes and improving of the results of IVM.

Over the years, several approaches have been used to evaluate COCs. Morphological evaluation is the main technique used to assess COC quality and to predict the subsequent maturation of oocytes in the IVM process. However, morphological evaluations are subjective and difficult, especially for COCs with

intermediate morphological qualities. Therefore, more objective evaluation criteria are needed. Previous studies have suggested that a greater understanding of the metabolic respiration of cumulus cells might yield new strategies for evaluating the quality of bovine oocytes [7, 8]. In this paper we describe the morphological evaluation of COCs and the application of a novel cell respiration measuring system using scanning electrochemical microscopy (SECM) to the assessment of the metabolic activity of cumulus cells and oocytes in bovine and human specimens.

Morphological Evaluation of Cumulus-oocyte Complexes and Oocytes

An appropriate evaluation of COCs is indispensable for the improvement of the IVM system, because cumulus cells play an important role in oocyte quality. For a morphologically precise evaluation of human COCs, size of an oocyte is an important parameter. The precise evaluation of human COCs is needed to predict the competence of oocyte maturation. Prior research has indicated that the diameter of immature oocytes is one of most reliable parameters for predicting oocyte quality. Eppig and Schroeder reported that mice oocytes isolated from females younger than 13 days of age are capable of spontaneous break down of the germinal vesicle (GVBD) when the mean diameter is greater than 60 μm [9]. In a study of porcine immature oocyte, progression to metaphase II was observed in 40% of oocytes that were over 110 μm in diameter, whereas no oocyte less than 90 μm in diameter resumed meiosis [10]. In rhesus monkey oocytes, in which meiotic competence occurs late during oocyte development, oocyte diameters appear relatively constant as the competence to undergo GVBD increases. These phenomena suggest that there is no association between oocyte diameter and maturation [11].

In comparison to animal systems, little is known about humans. Based on data from unstimulated polycystic ovary syndrome (PCOS) patients, Cavilla *et al.* deduced that an oocyte diameter of 81 μm at the time of retrieval was the threshold for GVBD, whereas oocytes of more than 103 μm would mature to metaphase II [12]. They also noted that, during *in vitro* human oocyte maturation, an increase in the average diameter of only 3 μm (from 106 to 109) represents a large change in the cytoplasmic volume (increasing an astonishing 8% during culture), suggesting that oocyte diameter provided valuable information about oocyte potential during IVM. In a proposal for the precise evaluation of human immature oocytes, the two-dimensional area of a depiction image was calculated using image analysis software "Image J".

Another important parameter of oocyte morphological quality is the volume of the human cumulus mass. During IVM, cumulus cells are known to maintain the oocyte nucleus at the GV stage [13]. Expanded human cumulus-oocyte complex patterns have a higher expression of LH receptor mRNA and are associated with more efficient oocyte maturation [14]. Early reports supported the idea that cumulus expansion during IVM improves the developmental capacity [15, 16]. In mice, the fertilization rate of IVM matured oocytes is correlated with the quantity and quality of the expanded cumulus mass [17]. The mechanical loss or spontaneous loss of cumulus cells from COCs has been shown to correlate with a loss of fertilizability [18]. Therefore, the quantity of cumulus mass is a factor influencing the success of IVM. For the morphological classification of cumulus mass, some researchers have separated the cumulus patterns into multilayered and expanded [19, 20].

In this review, we have estimated the multilayered and expanded cumulus mass as the consecutive change and made objective evaluations utilizing an image analysis software program. The COC area was calculated by tracing the edge of the cumulus mass. If the edge was not clear (usually observed in the expanded cumulus mass), the image was analyzed using an edge enhancement mode. The multiple layer formation of the cumulus mass was presented as the C-ratio (area of COC / area of immature oocyte). For the morphological evaluation of human COCs, forty-two human COCs, retrieved from eight women with the PCOS during an IVM program, were used. All COCs were aspirated 36 hours post-hCG between the 10th and 12th day of the menstrual cycle and cultured for 26 hours in TCM199 medium with 10% patient serum, 100 IU/L human chorionic gonadotropin and 75 IU/L follicle stimulating hormone under an atmosphere of 5% CO_2, 5% O_2, and 90% N_2. The parameters analyzed were (1) *Area*; area of the immature oocyte and (2) *Layer*; multiple layer formation of the cumulus mass, presented as the C-ratio. As shown in Fig. 1, these two morphological parameters were compared between the immature (germinal vesicle: GV or metaphase I: MI) and mature (metaphase II: MII) oocyte groups after *in vitro* culture. In the *Area* comparison, the mean level of *Area* was significantly higher in the mature group (8,886 ± 184 vs. 9,806 ± 161, Mean ± SEM, $P < 0.05$). In the

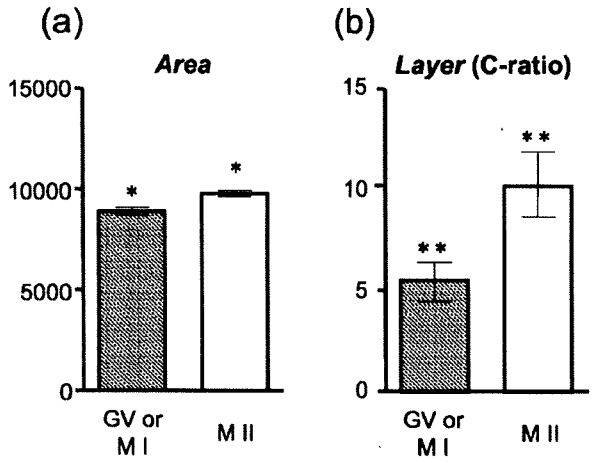

Fig. 1. Comparison of morphological parameters of human immature oocyte and COCs. a: *Area*, Area of immature oocyte; b: *Layer*, Multiple layer formation of cumulus mass was evaluated as C-ratio (Area of COC / Area of immature oocyte). Area and Layer were analyzed before *in vitro* culture and compared prospectively between mature (MII) and immature (MI or GV) group. *, **: significantly different ($P < 0.05$).

Layer comparison, the mean level of the C-ratio was significantly higher in the mature group (5.8 ± 0.8 vs. 10.3 ± 1.6, Mean ± SEM, $P < 0.05$). These results suggest the C-ratio is a useful parameter for predicting the maturation status of oocytes in the IVM process.

Subsequently, we examined the relationship between the cumulus mass morphology and the oocyte quality. Human COCs were classified into five grades based on cumulus mass morphology as follows: Grade 1 (G1), cumulus cells with multi-layers covering the whole oocyte, and a regular round oocyte; Grade 2 (G2), cumulus cells with multi-layers (less than three layers), covering the whole oocyte and a regular round oocyte; Grade 3 (G3), regular round oocytes with cumulus cells covering half of the domain; Grade 4 (G4), naked oocytes without cumulus mass; Grade 5 (G5), naked and irregular shaped oocytes (Fig. 2). High maturation rates of immature oocytes were detected in G1 and G2 (70.0% and 64.3%, respectively) in contrast to the lower maturation rate of 17.7% (mean percentage from G3 to G5).

Cumulus cells are a production site of steroids, growth factor, proteins and other compounds that contribute to cytoplasmic maturation of oocytes. Beneficial effects of cumulus cells on microtubule dynamics and/or chromatin stability, oocyte maturation and early embryonic development have been reported in many species, including humans [21–23]. Cumulus cells are also known to play an important role in the regulation of the meiotic progression of oocytes. During the growth and development of meiotic competence of an oocyte, the cumulus cells are responsible for maintenance of nuclear arrest at the germinal vesicle (GV) stage by transfer of an inhibitory signal through gap junctions which elevates the intracellular cyclic adenosine monophosphate (cAMP) level in the oocytes

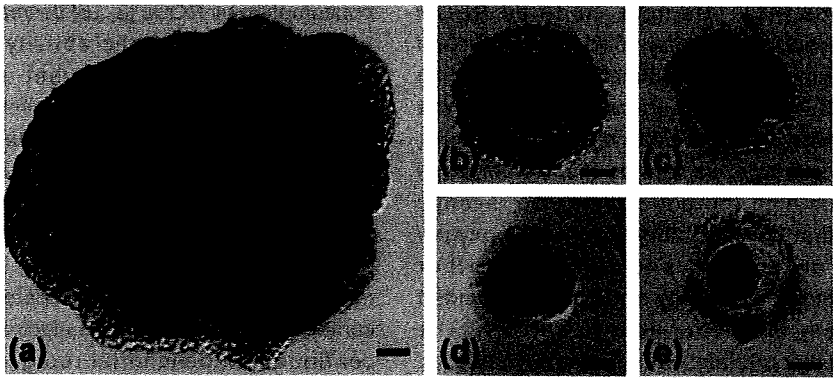

Fig. 2. Light micrographs of human COCs classified by morphological evaluation. (a) Grade 1, cumulus cells with multi-layers covering the whole oocyte, and a regular round oocyte; (b) Grade 2, cumulus cells with multi-layers (less than three layers), covering the whole oocyte and a regular round oocyte; (c) Grade 3, regular round oocytes with cumulus cells covering half of the domain; (d) Grade 4, naked oocytes without cumulus mass; (e) Grade 5, naked and irregular shaped oocytes. Bars = 20 μm.

[24, 25]. Although the precise regulation mechanism of meiotic progression is still controversial [26], it has been suggested that well-developed cumulus cells have the capacity to regulate appropriate maturation and the development of immature oocytes.

Evaluating the Quality of Embryos and Oocytes with Measurement of Respiration Activity with an Electrochemical Measuring Technique

The metabolic activity of embryos and oocytes has been determined from the consumption of nutrients, such as glucose, pyruvate and amino acids [27–30]. Oxygen consumption is an idea indicator of overall metabolic activity because adenosine triphosphate (ATP) is predominantly generated by oxidative phosphorylation, a process in which oxygen plays an essential role [31–33]. Oxygen consumption by embryos and oocytes has been studied with various measuring techniques, such as the Cartesian diver [34, 35], spectrophotometry [36, 37], ultrafluorescence measurements [38, 39], and self-referencing microelectrodes [40–43].

Electrochemical measurement using scanning electrochemical microscopy (SECM) is a technique in which the tip of a microelectrode monitors the local distribution of electro-active species, such as oxygen near the sample surface [44]. This technique can measure the concentration profile of a metabolic product around a spherical sample, such as an embryo, with a probe microelectrode. We have employed the SECM technique to examine oxygen consumption by single embryos [45]. Using a modified SECM measuring procedure, we quantified the respiration activity of embryos in several animal species including humans [46]. SECM can non-invasively measure the respiration activity of single embryos from livestock, such as cattle and pigs, as well as those from small rodents, all with high reproducibility. We recently demonstrated that bovine embryos with high oxygen consumption are better candidates for further development into good quality embryos and yielded higher pregnancy rates after embryo transfer. The respiration activity correlates with the embryo quality. SECM is a highly sensitive and non-invasive method for measuring cellular respiration and may be a valuable tool for accurately assessing the quality of embryos, which could contribute to improved outcomes in assisted reproduction, including human IVF. On the other hand, an accurate method for evaluating the respiratory activity of oocytes remains to be developed.

Table 1. Oxygen consumption rates ($F \times 10^{14}$/mol · s^{-1}) of bovine COCs and denuded oocytes in oocyte maturation cultures

Maturation status	COC (n)	Oocyte (n)
Immature	5.48 ± 0.82 (16)^{a}	0.67 ± 0.02 (16)^{c}
Mature	3.15 ± 0.42 (20)^{b}	1.10 ± 0.05 (20)^{d}

Values with different superscripts in each column differ significantly ($P < 0.05$).

Oocyte quality could be the most important factor in determining successful fertilization and embryo development. Therefore, we attempted to establish an evaluation system for oocyte quality based on the respiratory activity of oocytes.

In previous studies, we evaluated the SECM technique, to establish an accurate method for measuring the respiratory activity of single bovine and porcine oocytes [8, 48]. With the SECM procedure, oxygen consumption of bovine COCs and denuded oocytes was monitored (Table 1). Oxygen consumption rates ($\times 10^{14}$/mol · s^{-1}) of immature COCs and oocytes (immediately after recovery from an ovary) were 5.48 and 0.67, respectively. Although the respiration rate of denuded oocytes was lower than that of cumulus cells, the oxygen consumption rate by a single bovine oocyte was quantitatively measured by SECM.

Oxygen consumption has been monitored in COCs and oocytes cultured in serum-free medium for oocyte maturation. An increase in the oxygen consumption rate was found in oocytes [1, 10], whereas the oxygen consumption by COCs [3, 15] decreased during IVM. To analyze the metabolic activity of mitochondrial respiration, the ATP content and mitochondrial distribution in oocytes were examined. The ATP content of oocytes after maturation culture was significantly higher than that of immature oocytes (Fig. 3). In immature oocytes, staining with MitoTracker Orange revealed mitochondrial clumps with a strong signal in the periphery of the cytoplasm (Fig. 4). After IVM, the mitochondrial clumps were located more toward the center of the cytoplasm. An electron microscope study confirmed mitochondrial reorganization in bovine oocytes during oocyte maturation (Fig. 5). These results show that the respiratory activity of bovine oocytes increases during IVM and mitochondrial reorganization may thus be partly due to the respiratory activity. Therefore, we consider the SECM procedure is a useful technique for evaluating the metabolic activity and quality of single oocytes.

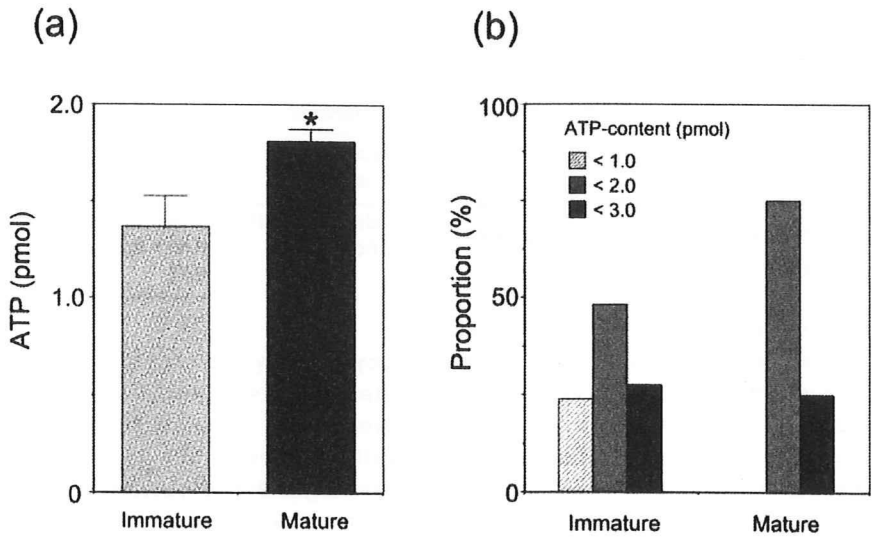

Fig. 3. (a) The ATP content and (b) proportion of oocytes categorized by ATP content: immature and mature bovine oocytes. *: significantly different ($P < 0.05$).

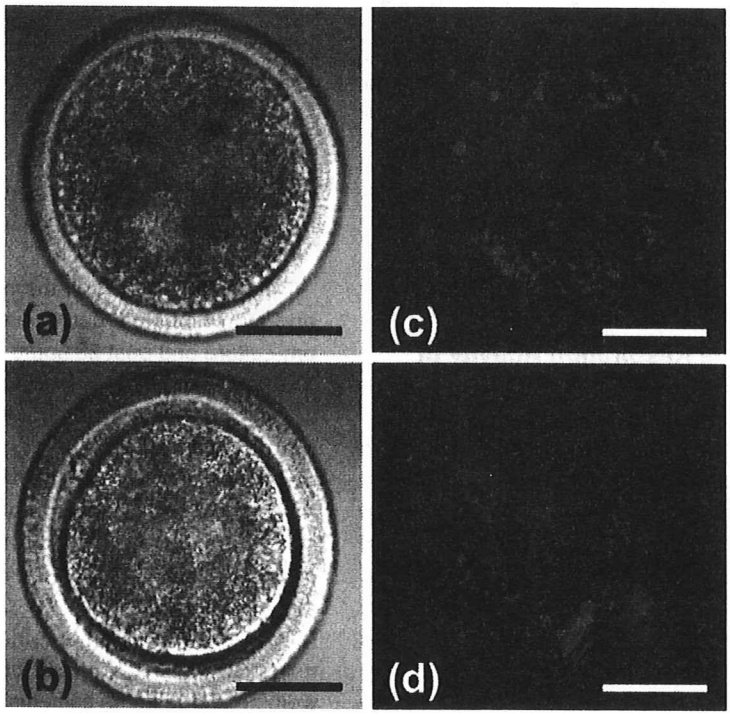

Fig. 4. Midline confocal sections of (a, b) immature and (c, d; cultured in IVMD101 medium) mature bovine oocytes stained by MitoTracker orange. Bars = 50 μm.

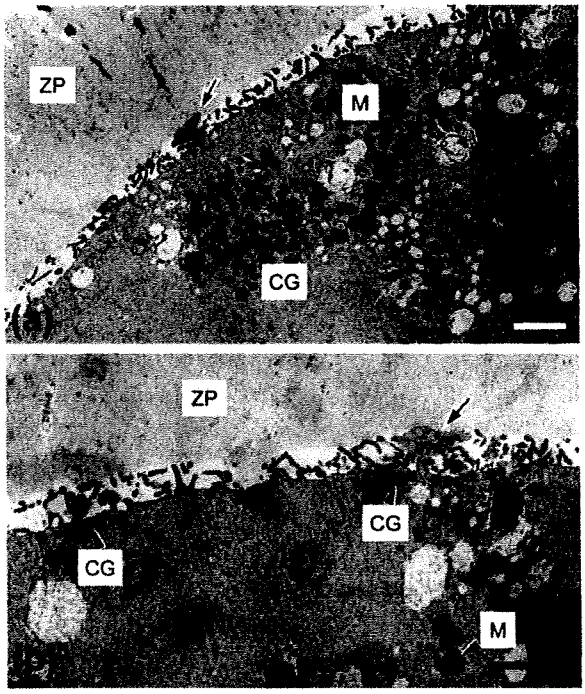

Fig. 5. Electron micrographs of (a) immature and (b) cultured in serum-free maturation medium mature oocytes. a: Many aggregates of mitochondria (M) and cortical granules (CG) were present in the cortex cytoplasm. b: Cortical granules were distributed in the periphery of the cytoplasm, but aggregates of mitochondria were not found. ZP, zona pellucida. Arrows: microvilli. Bars = 2 μm.

Table 2. Oxygen consumption rates ($F \times 10^{14}$/mol · s^{-1}) of human COCs classified by morphological evaluation

Category	Pre-culture (n)	Post-culture (n)
G1	7.79 ± 1.00 (50)	6.11 ± 0.74 (50)
G2	1.46 ± 0.15 (25)	1.63 ± 0.33 (25)
G3	1.26 ± 0.35 (8)	1.60 ± 0.55 (8)
G4	0.86 ± 0.30 (2)	0.79 ± 0.11 (2)
G5	0.77 (1)	0.35 (1)

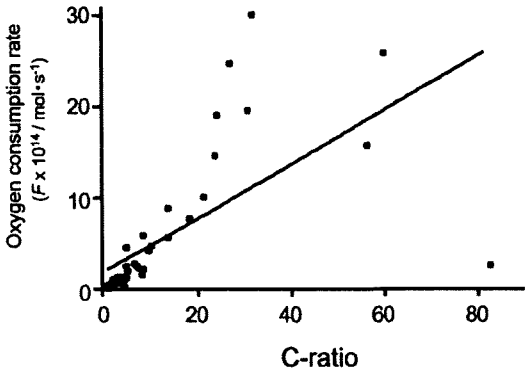

Fig. 6. Correlation between oxygen consumption rate and C-ratio.

Measuring the Respiration Activity of Human COCs and Oocytes

In this part, we review the respiration activity of human COCs and oocytes. Eighty-five human COCs retrieved from eighteen women with the PCOS during an IVM program were examined. Informed consent for the use of the COCs in this study was obtained from all the patients. Thirteen of the eighteen women were administered a short course of follicular stimulating hormone (FSH) and five women accomplished an IVM program without the use of FSH before hCG administration. All COCs were aspirated 36 h post-hCG between the 10th and 12th day of the menstrual cycle and cultured 26 h in TCM199 medium with 10% patient serum, 100 IU/L human chorionic gonadotropin and 75 IU/L follicle stimulating hormone under an atmosphere of 5% CO_2, 5% O_2, and 90% N_2. Cellular unevenness of the cumulus mass has an influence on SECM measurement results. Therefore, the oxygen consumption rate was measured three times for each COC and the mean was used as the measured value.

Relationship between the oxygen consumption rates and morphological categories of human COCs in the pre-culture and post 26 hours-culture stages is shown in Table 2. A linear correlation between the oxygen consumption rate and the C-ratio was shown in Fig. 6 (correlation coefficient: $r^2 = 0.423$, $P < 0.01$). The respiration activity measured by SECM showed that the respiration activity of human COCs with multi-layer cumulus cells (G1) was higher than in the other categories (G2–G5). Ultrastructual studies revealed that the cumulus cells in G1 COCs, which showed high respiration activity, contained many well-developed mitochondria. In contrast, undeveloped mitochondria were scattered in the cumulus cells in G3 COCs (Fig. 7). These results suggest that respiration rates are directly influenced by the surrounding cumulus volume and mitochondrial activity in cumulus cells.

A comparison of the oxygen consumption fluctuation between the pre-culture stage and after 26 hours of culture is shown in Fig. 8. In the FSH administration group, the mean oxygen consumption rate tended to

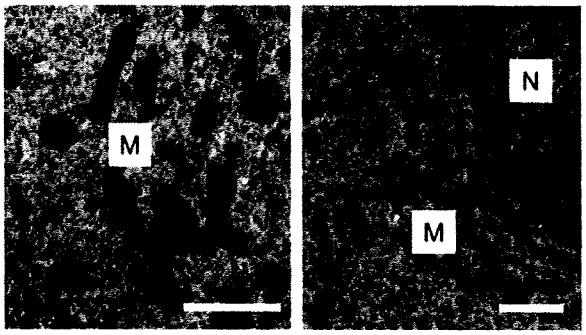

Fig. 7. Electron micrographs of human cumulus cells. Many well-developed mitochondria (M) are present in the cumulus cells of the Grade 1 COC (left image). In contrast, mitochondria showing small size are scattered in the cumulus cells of the Grade 3 COC. N: Nucleus. Bars = 1 μm.

decrease after 26 h of culture (5.62 ± 0.83 vs. 4.25 ± 0.58). In contrast, the mean oxygen consumption rates were similar between the two stages in the non-FSH administration group (4.07 ± 1.19 vs. 4.17 ± 1.02). There was no clinical advantage gained by extending the FSH pre-treatment from 3 to 6 days to produce follicles more than 10 mm in diameter [49]. On the other hand, Wynn *et al.* demonstrated a higher maturation rate in a FSH treatment group [50]. In their study, the maturation rate to metaphase II was higher in the FSH administration group (68.3% vs. 61.3%, in comparison to the non-FSH administration group, unpublished data). The benefit of FSH pre-treatment remains controversial and the development competence cannot be evaluated because of the limitations of the current study protocol.

The efficacy of the administration of hCG remains controversial. In hCG protocol, all patients are administered hCG before oocyte retrieval. After the LH surge, oocytes resume the first meiotic division and enter the second division [51]. At the same time, cumulus mass begins to change to the expanding form. Cumulus expansion may influence a variety of fundamental developmental changes which occur during fertilization. Regarding the use of hCG in bovine, the cumulus cells from antral follicles as small as 5 mm have mRNA transcripts for LH receptors and may respond to hCG stimulation [52]. This finding provides evidence of a mechanism by which hCG begins the maturation process of small antral oocytes *in vivo* and facilitates the completion of meiosis *in vitro*. Chian *et al.* demonstrated that the percentage of oocytes achieving maturation after 48 h *in vitro* culture was significantly higher in the hCG-primed group than in the non-hCG-primed group during human IVM-IVF [53].

Finally, the results of the respiration measurement of single human oocytes using a SECM system are listed in Table 3. The oxygen consumption rate of pre-cultured oocytes (GV stage) was 0.49 × 10^{14}/mol · s^{-1},

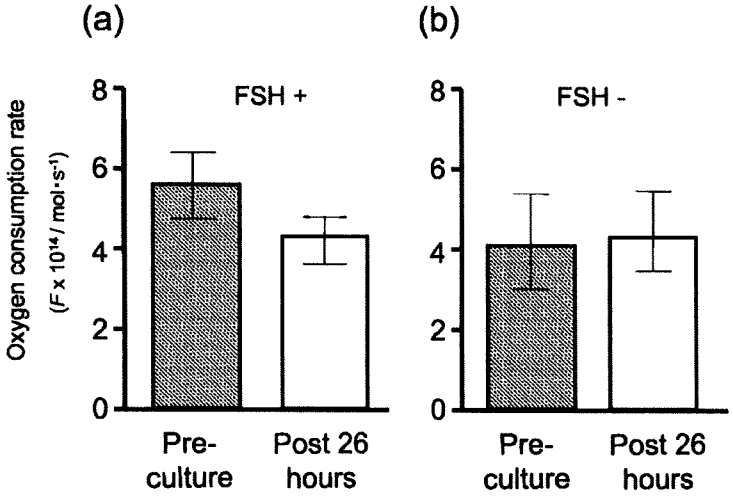

Fig. 8. Comparison of oxygen consumption with or without FSH administration at the pre-culture stage and after 26 h of culture. (a) oxygen consumption rate in the FSH administered group and (b) in the non-FSH administered group.

Table 3. Oxygen consumption rates ($F \times 10^{14}$/mol · s^{-1}) of human denuded oocytes in oocyte maturation cultures

Maturation status	Oxygen consumption rate (n)
GV (Pre-culture)	0.49 ± 0.07 (10)
GV or MI (Post-culture)	0.40 ± 0.21 (19)
MII (Post-culture)	0.41 ± 0.15 (30)

whereas the oxygen consumption rate tended to decrease in matured MII oocytes (0.41 × 10^{14}/mol · s^{-1}). These results suggest that the respiration activity of human oocytes changes with maturation status of oocytes, although the mechanism of this fluctuation needs to be confirmed with further studies.

Conclusions

The SECM technique is a non-invasive and sensitive method for measuring the oxygen consumption of individual COCs and oocytes in animal species including humans. The respiration activity of COCs is directly influenced by the surrounding cumulus cell volume and the mitochondrial activity of cumulus cells. Biochemical and cytological studies strongly suggest that oxygen consumption is an important parameter for evaluating the competence of oocyte maturation. It may be feasible to monitor the profile of an oocyte's mitochondrial activity by measureing its oxygen consumption, and select the oocytes that can sustain fertilization and the development of embryos. Therefore, the SECM technique may have a future in clinical application as a predictor of oocyte quality which could be used for determining to develop into good quality embryos.

Acknowledgements

This work was supported by Research and Development Program for New Bio-Industry Initiatives, Bio-oriented Technology Research Advancement Institution (BRAIN), Grant-in-Aid for Scientific Research (17380164), on Priority Areas "Lifesurveyor" (19021006) from the Ministry of Education, Culture, Sports, Science and Technology of Japan, Special Coordination Funds for Promoting Science and Technology of Japan, and the Japan Livestock Technology Association.

References

1) Blondin, P., Bousqent, D., Twagiramungu, H., Barnes, F. and Sirand, M.A. (2002): Manipulation of follicular development to produce developmentally competent bovine oocyte. Biol. Reprod., 66, 38–43.
2) Barnes, F.L. and Sirard, M.A. (2000): Oocyte maturation. Semin. Reprod. Med., 18, 123–131.
3) Cha, K.Y., Koo, J.J., Ko, J.J., Choi, D.H., Han, S.Y. and Yoon, T.K. (1991): Pregnancy after in vitro fertilization of human follicular oocytes collected from nonstimulated cycles, their culture in vitro and their transfer in a donor oocyte program. Fertil. Steril., 55, 109–113.
4) Le Du, A., Kadoch, I.J., Bourcigaux, N., Doumerc, S., Bourrier, M.C., Chevalier, N., Fanchin, R., Chian, R.C., Tachdjian, G., Frydman, R. and Frydman, N. (2005): In vitro maturation for the treatment of infertility associated with polycystic ovarian syndrome: the French experience. Hum. Reprod., 20, 420–424.
5) Soderstrom-Anttila, V., Makinen, S., Tuuri, T. and Suikkari, A.M. (2005): Favorable pregnancy results with insemination of in vitro matured oocytes from unstimulated patients. Hum. Reprod., 20, 1534–1540.
6) Nagai, T. (2001): The improvement of in vitro maturation systems for bovine and porcine oocytes. Theriogenology, 55, 1291–1301.
7) Abe, H., Saito, T., Shiku, H., Yokoo, M., Itoh-Sasaki, T., Hoshi, H. and Matsue, T. (2006): Analysis of respiratory activity of single bovine oocytes by scanning electrochemical microscopy. In: Proceeding of the 4th International Forum on Post-genome Technologies, pp. 19–22.
8) Abe, H., Shiku, H., Aoyagi, S., Matsue, T. and Hoshi, H. (2006): Oxygen consumption of bovine cumulus cells and oocytes cultured in different culture systems for oocyte maturation. Reprod. Fertil. Dev., 18, 267.
9) Eppig, J.J. and Schroeder, A.C. (1989): Capacity of mouse oocytes from preantral follicles to undergo embryogenesis and development to live young after growth, maturation and fertilization in vitro. Biol. Reprod., 41, 268–276.
10) Hirao, Y., Nagai, T., Kubo, M., Miyano, T., Miyake, M. and Kato, S. (1994): In vitro growth and maturation of pig oocytes. J. Reprod. Fertil., 100, 333–339.
11) Schramm, R.D., Tennier, M.T., Boatman, D.E. and Bavister, B.D. (1993): Chromatin configuration and meiotic competence of oocytes are related to follicular diameter in non-stimulated rhesus monkeys. Biol. Reprod., 48, 349–356.
12) Cavilla, J.K., Kennedy, C.R., Byskov, A.G. and Hartshorne, G.M. (2008): Human immature oocytes grow during culture for IVM. Hum. Reprod., 23, 37–45.
13) Dekel, N. and Beers, W.H. (1980): Development of the rat oocyte in vitro: Inhibition and induction of maturation in the presence or absence of the cumulus oophorus. Dev. Biol., 75, 247–254.
14) Yang, S.H., Son, W.Y., Yoon, S.H., Ko, Y. and Lim, J.H. (2005): colleration between in vitro maturation and

expression of LH receptor in cumulus cells of the oocytes collected from PCOS patients in HCG-primed IVM cycles. Hum. Reprod., 20, 2097–2103.
15) Ball, G.D., Leibfried, M.L., Lenz, R.W., Ax, R.L., Bavister, B.D. and First, N.L. (1983): Factors affecting successful in vitro fertilization of bovine follicular oocytes. Biol. Reprod., 28, 717–725.
16) Naito, K., Fukuda, Y. and Toyama, Y. (1988): Effects of porcine follicular fluid on male pronucleus formation in porcine oocytes matured in vitro. Gamete. Res., 21, 289–295.
17) Chen, L., Russell, P.T. and Larsen, W.J. (1993): Functional significance of cumulus expansion in the mouse: Roles for the preovulatory synthesis of hyaluronic acid within the cumulus mass. Mol. Reprod. Dev., 34, 87–93.
18) Itagaki, Y. and Toyoda, Y. (1991): Factors affecting fertilization in vitro of mouse eggs after removal of cumulus oophorus. J. Mamm. Ova Res., 8, 126–134.
19) Smitz, J., Picton, H.M., Platteau, P., Rutherford, A., Cortvrindt, R., Clyde, J., Nogueira, D., Devroey, P., Lyby, K. and Grondahl, C. (2007): Principal findings from a multicenter trial investigating the safety of follicular-fluid meiosis-activating sterol for in vitro maturation of human cumulus- enclosed oocytes. Fertil. Steril., 87, 949–964.
20) Jurema, M.W. and Noguera, D. (2006): In vitro maturation of human oocytes for assisted reproduction. Fertil. Steril., 86, 1277–1291.
21) Cha, K.Y. and Chian, R.C. (1998): Maturation in vitro of human oocytes for clinical use. Hum. Reprod. Update., 4, 103–120.
22) Goud, P.T., Goud, A.P., Qian, C., Laverge, H., Van der Elst, J., De Sutter, P. and Dhout, M. (1998). In vitro maturation of human germinal vesicle stage oocytes: role of cumulus cells and epidermal growth factor in the culture medium. Hum. Reprod., 13, 1638–1644.
23) Ueno, S., Kurome, M., Ueda, H., Tomii, R., Hiruma, K. and Nagashima, H. (2005): Effects of maturation conditions on spindlemorphology in porcine MII oocytes. J. Reprod. Dev., 51,405–410.
24) Isobe, N. and Terada, T. (2001): Effect of the factor inhibiting germinal vesicle breakdown on the disruption of gap junctions and cumulus expansion of pig cumulus-oocyte complexes cultured in vitro. Reproduction, 121, 249–257.
25) Tanghe, S., Van Soom, A., Nauwynck, H., Coryn, M. and De Kruif, A. (2002): Minireview: Functions of the cumulus oophorus during oocyte maturation, ovulation and fertilization. Mol. Reprod. Dev., 61, 414–424.
26) Guoliang, X., Byskov, A.G. and Anderson, C.Y. (1994): Cumulus cells secrete a meiosis-inducing substance by stimulation with forskolin and cyclic adenosine monophosphate. Mol. Reprod. Dev., 39, 17–24.
27) Rieger, D. (1992): Relationship between energy metabolism and development of early mammalian embryos. Theriogenology, 37, 75–93.
28) Rieger, D., Loskutoff, N.M. and Betteridge, K.J. (1992): Developmentally related changes in the uptake and metabolism of glucose, glutamine and puruvate by cattle embryos produced in vitro. Reprod. Fertil. Dev., 4, 547–557.
29) Rieger, D. and Loskutoff, N.M. (1994): Changes in the metabolism of glucose, puruvate, glutamine and glycine during maturation of cattle oocytes in vitro. J. Reprod. Fertil., 100, 257–262.
30) Gopichandran, N. and Leese, H.J. (2003): Metabolic characterization of the bovine blastocyst, inner cell mass, trophectoderm and blastocoel fluid. Reproduction, 126, 299–308.
31) Thompson, J.G., Partridge, R.J., Houghton, F.D., Cox, C.I. and Leese, H.J. (1996): Oxygen uptake and carbohydrate metabolism by in vitro derived bovine embryos. J. Reprod. Fertil., 106, 299–306.
32) Thompson, J.G., McNaughton, C., Gasparrini, B., McGowan, L.T. and Tervit, H.R. (2000): Effect of inhibitors and uncouplers of oxidative phosphorylation during compaction and blastulation of bovine embryos cultured in vitro. J. Reprod. Fertil., 118, 47–55.
33) Trimarchi, J.R., Liu, L., Porterfield, D.M., Smith, P.J.S. and Keefe, D.L. (2000): Oxidative phosphorylation-dependent and -independent oxygen consumption by individual preimplantation mouse embryos. Biol. Reprod., 62, 1866–1874.
34) Fridhandler, I., Hafez, E.S.E. and Poncus, G. (1957): Developmental changes in the repiratory activity of rabbit ova. Experiments in Cell Research, 13, 132–139.
35) Mills, R.M. and Brinster, R.L. (1967) Oxygen consumption of preimplantation mouse embryos. Exp. Cell Res., 470, 337–344.
36) Magnusson, C., Hillensjo, T., Hamberger, L. and Nilsson, L. (1986): Oxygen consumption by human oocytes and blastocysts grown in vitro. Hum. Reprod., 1, 183–184.
37) Nilsson, B., Magnusson, C., Widehn, S. and Hillensjo, T. (1982): Correlation between blastocyst oxygen consumption and trophoblast cytochrome oxidase reaction at initiation of implantation of delayed mouse blastocysts. J. Embryol. Exp. Morphol., 71, 75–82.
38) Houghton, F.D., Thompson, J.G., Kennedy, C.J. and Leese, H.J. (2000): Oxygen consumption and energy metabolism of the early mouse embryo. Mol. Reprod. Dev., 44, 476–485.
39) Trimarchi, J.R., Liu, L., Smith, P.J.S. and Keefe, D.L. (2000): Noninvasive measurement of potassium efflux as an early indicator of cell death in mouse embryos. Biol. Reprod., 63, 851–857.
40) Land, S.C., Porterfield, D.M., Sanger, R.H. and Smith, P.J.S. (1999): The self-referencing oxygen-selective microelectrode: detection of transmembrane oxygen flux from single cells. J. Exp. Biol., 202, 211–218.
41) Smith, P.J.S., Hammar, K., Porterfield, D.M., Sanger, R.H. and Trimarchi, J.R. (1999): Self-referencing, non-invasive, ion selective electrode for single cell detection of trans-plasma membrane calcium flux. Microsc. Res. Tech., 46, 398–417.
42) Lopes, A.S., Larsen, L.H., Ramsing, N., Lovendahl, P.,